Research Square

Preprints are preliminary reports that have not undergone peer review.
They should not be considered conclusive, used to inform clinical practice,
or referenced by the media as validated information.

Efficient Charging of Nuclear Quantum Batteries via Chain-STIRAP: A Five-State Ladder System with XFEL Pulses

Reza Gholizadeh Ahmadabadi
Islamic Azad University Ardabil
Bashir Nedaee-Shakarab
nedaei829@iau.ac.ir

Islamic Azad University Ardabil
Hossein Akbari
Islamic Azad University Ardabil
Naser Shirkhanghah
Islamic Azad University

Research Article

Keywords: Quantum battery, Ergotropy, Chain-STIRAP, Nuclear states, XFEL

Posted Date: November 9th, 2026

DOI: https://doi.org/10.21203/rs.3.rs-11368002/v1

License: This work is licensed under a Creative Commons Attribution 4.0 International License.
Read Full License

Additional Declarations: No competing interests reported.

Efficient Charging of Nuclear Quantum Batteries via Chain-STIRAP: A Five-State Ladder System with XFEL Pulses

Reza Gholizadeh Ahmadabadi, Bashir Nedaee-Shakarab,* and Hossein Akbari
Department of Physics, Ard.C., Islamic Azad University, Ardebil, Iran.

Naser Shirkhanghah
Department of Physics, Kha.C., Islamic Azad University, Khalkhal, Iran.
(Dated: October 13, 2026)

We propose an efficient scheme for charging a quantum battery based on a five-state ladder-type nuclear system using the chain-STIRAP technique. Four time-delayed X-ray free-electron laser pulses interact with an accelerated nuclear beam, where the relativistic Doppler effect compensates the frequency mismatch between gamma-ray transitions and laser photons. Using ^{168}Er as a realistic example, we demonstrate complete population transfer from $|1\rangle$ to $|5\rangle$ without populating intermediate states. In addition to population dynamics, we calculate the stored energy and ergotropy as key performance metrics for quantum battery applications. A three-state system is also analyzed for comparison. Our results show that the final ergotropy reaches 99% of the stored energy for the five-state system, compared to 95% for the three-state case. The charging efficiency exceeds 0.98 under optimal pulse conditions, while the required peak laser intensity is about 10^{26} W/cm^2, considerably lower than conventional π-pulse or STIRAP protocols. This work establishes chain-STIRAP as a viable tool for high-density energy storage in nuclear quantum batteries.
Keywords: Quantum battery, Ergotropy, Chain-STIRAP, Nuclear states, XFEL.

I. INTRODUCTION

The interaction of laser fields with quantum systems enables precise control over population distribution among discrete energy levels. This capability has found widespread applications in atomic and molecular physics, quantum information processing, and precision metrology [1–3]. Among various coherent control techniques, stimulated Raman adiabatic passage (STIRAP) has emerged as a powerful method for complete population transfer between two quantum states without populating intermediate levels [4–6]. The robustness of STIRAP against parameter fluctuations and its immunity to spontaneous emission from excited states make it particularly attractive for practical implementations.

The success of STIRAP in three-level systems has motivated its extension to more complex multilevel configurations. Chain-type systems, where states are coupled sequentially as $|1\rangle \leftrightarrow |2\rangle \leftrightarrow \cdots \leftrightarrow |N\rangle$, have been theoretically investigated [7]. It has been shown that for odd N, the Hamiltonian possesses a dark state that excludes even-numbered states, enabling direct population transfer from $|1\rangle$ to $|N\rangle$ under appropriate pulse sequences. This generalized scheme, known as chain-STIRAP, has been successfully implemented in various atomic and molecular systems [8–10].

Recent advances in X-ray free-electron laser (XFEL) technology have opened new opportunities for studying coherent light-matter interactions in the nuclear regime [11–13]. Nuclear states offer significantly larger transition energies compared to atomic systems, making them attractive for high-density energy storage applications. However, the frequency of existing XFEL sources is typically lower than typical gamma-ray transition frequencies. This obstacle can be overcome by accelerating the nuclear beam and exploiting the relativistic Doppler effect, which shifts the observed laser frequency in the nuclear rest frame [14].

Several studies have applied coherent population transfer techniques to nuclear systems. The π-pulse method was first demonstrated for two-level nuclei using relativistic Doppler compensation [14]. Subsequently, the STIRAP technique was extended to three-level Λ-type and ladder-type nuclear configurations [15, 16]. To reduce the required laser intensity, optimized schemes such as composite STIRAP and train of coincident pulses have been proposed [17–19]. More recently, the chain-STIRAP technique was successfully implemented in a five-state ladder-type nuclear system using ^{168}Er as a testbed, demonstrating complete population transfer from $|1\rangle$ to $|5\rangle$ [20].

Quantum batteries represent a novel paradigm for energy storage that leverages quantum mechanical principles such as superposition and entanglement [21–23]. Unlike classical electrochemical batteries, quantum batteries store energy in discrete quantum states and can achieve higher power densities through collective charging effects [24–26]. A key figure of merit for quantum batteries is ergotropy, defined as the maximum amount of work that can be extracted from a quantum system by cyclic unitary operations *Alicki2013, Hovhannisyan2013*. While ergotropy has been extensively studied in atomic and spin-based quantum battery systems [28–30], its application to nuclear systems remains largely unexplored.

In this paper, we bridge the gap between nuclear coherent population transfer and quantum battery tech-

* nedaei829@iau.ac.ir

nology. We investigate the optimization of stored energy and ergotropy in a five-state ladder-type nuclear system charged via the chain-STIRAP protocol. A three-state system is also analyzed as a benchmark for comparison. Using ^{168}Er nuclear parameters and realistic XFEL specifications, we demonstrate that chain-STIRAP enables high-efficiency charging with near-maximal ergotropy while requiring significantly lower laser intensities than conventional methods. The paper is organized as follows. Section 2 presents the theoretical model including the relativistic Doppler condition and the chain-STIRAP Hamiltonian. Section 3 defines the quantum battery performance metrics. Section 4 presents numerical results for both three-state and five-state systems. Section 5 concludes the paper.

II. THEORETICAL FRAMEWORK

A. Relativistic Doppler compensation for nuclear resonance

A major obstacle in driving nuclear transitions with XFEL pulses is the frequency gap between typical gamma-ray transitions (keV to MeV range) and available XFEL photon energies (up to tens of keV). To overcome this limitation, we consider a beam of nuclei moving with relativistic velocity toward the XFEL source.

For a nucleus moving with speed $v = \beta c$, the observed frequency in the nuclear rest frame is shifted via the relativistic Doppler effect:

$$\omega_{\rm obs} = \gamma(1+\beta)\omega_L, \tag{1}$$

where $\gamma = 1/\sqrt{1-\beta^2}$ is the Lorentz factor and ω_L is the laser frequency in the laboratory frame. For a multi-level ladder-type nuclear system with states $|1\rangle, |2\rangle, \ldots, |N\rangle$, the resonance condition for each transition $|i\rangle \leftrightarrow |j\rangle$ is:

$$\gamma(1+\beta)\omega_{ij}^{(L)} = \omega_{ij}^{(obs)}, \tag{2}$$

where $\omega_{ij}^{(obs)} = (E_j - E_i)/\hbar$ is the nuclear transition frequency. For the copropagating scheme where all laser beams travel parallel to the nuclear beam, for each pulse, we have to use different laser frequency. An alternative approach uses a single laser frequency ω_L for all pulses, with each pulse impinging on the nuclear beam at a different angle θ_{ij}. The resonance conditions become:

$$\gamma(1+\beta\cos\theta_{ij})\omega_L = \omega_{ij}^{(obs)}, \tag{3}$$

B. The three-state system

We first consider a three-state ladder-type nuclear system as shown in Fig. 1. The states $|1\rangle$, $|2\rangle$, and $|3\rangle$ are coupled sequentially via two XFEL pulses. The pump pulse couples $|1\rangle \leftrightarrow |2\rangle$ and the Stokes pulse couples $|2\rangle \leftrightarrow |3\rangle$. This three-state configuration serves as a benchmark for understanding the fundamental principles of STIRAP before extending to the five-state system.

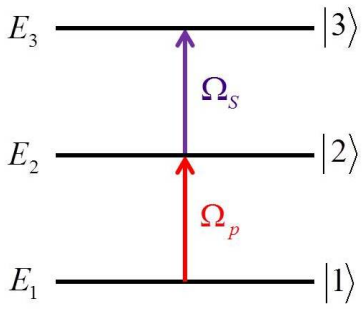


FIG. 1. Linkage pattern for a three-state ladder-type nuclear system. The states $|1\rangle$ to $|3\rangle$ are coupled sequentially by two XFEL pulses with Rabi frequencies Ω_p, and Ω_S. All transitions are resonantly driven under the relativistic Doppler condition.

Within the rotating wave approximation and in the interaction picture, the Hamiltonian for the three-state system takes the form:

$$H^{(3)}(t) = \frac{\hbar}{2}\begin{pmatrix} 0 & \Omega_p(t) & 0 \\ \Omega_p(t) & 0 & \Omega_S(t) \\ 0 & \Omega_S(t) & 0 \end{pmatrix}, \tag{4}$$

where $\Omega_p(t)$ and $\Omega_S(t)$ are the time-dependent Rabi frequencies associated with the pump and Stokes pulses. The zero diagonal elements indicate that all transitions are resonantly driven with zero detuning under the Doppler condition. The resonance conditions are assumed as follow:

$$\gamma(1+\beta\cos\theta_p)\omega_p = \omega_{12}, \tag{5}$$
$$\gamma(1+\beta\cos\theta_S)\omega_S = \omega_{23}. \tag{6}$$

Figure 2 schematically shows the interaction of an accelerated three-state nuclear beam with two XFEL pump and Stokes pulses in the crossed-beam configuration. The pump pulse with angle $\theta_p = 0$ couples $|1\rangle \leftrightarrow |2\rangle$, and the Stokes pulse at angle θ_S couples $|2\rangle \leftrightarrow |3\rangle$. The relativistic Doppler shift brings all laser frequencies into resonance with their respective nuclear transitions.

A cornerstone of the STIRAP technique is the existence of a dark state, which is an eigenstate of the Hamiltonian with zero eigenvalue that contains no contribution from the excited state $|2\rangle$:

$$|\Phi^{(0)}(t)\rangle = \cos\theta(t)|1\rangle - \sin\theta(t)|3\rangle, \tag{7}$$

where the mixing angle is defined as $\tan\theta(t) = \Omega_p(t)/\Omega_S(t)$. This state contains no contribution from $|2\rangle$ regardless of the values of Ω_p and Ω_S. This is the key feature enabling population transfer without populating the intermediate level, thereby avoiding spontaneous emission losses from $|2\rangle$.

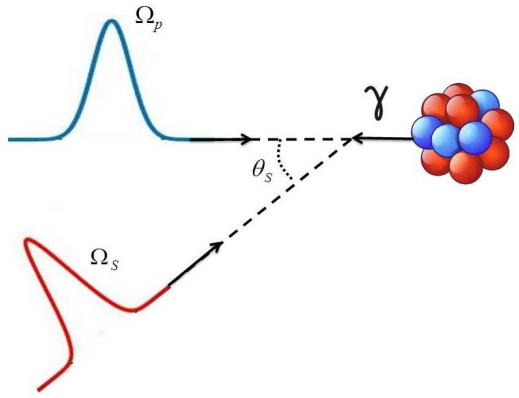


FIG. 2. Schematic of an accelerated nuclear beam interacting with two XFEL pulses in the crossed-beam configuration. Each laser pulse makes a different angle $\theta_{p(S)}$ with the nuclear beam direction, allowing a single laser frequency to drive multiple nuclear transitions via the angle-dependent relativistic Doppler shift.

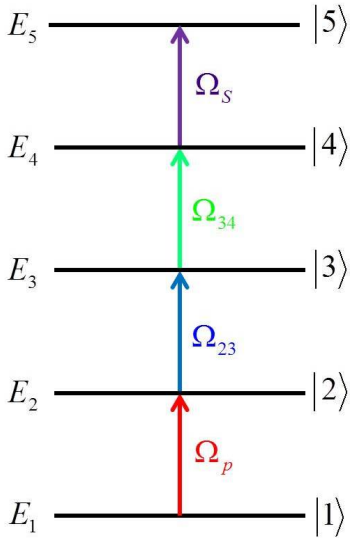


FIG. 3. Linkage pattern for a five-state ladder-type nuclear system. The states $|1\rangle$ to $|5\rangle$ are coupled sequentially by two XFEL pulses with Rabi frequencies Ω_p, Ω_{23}, Ω_{34}, and Ω_S. All transitions are resonantly driven under the relativistic Doppler condition.

According to the adiabatic theorem, if the system is initially in an eigenstate and the Hamiltonian varies sufficiently slowly, the system will remain in that eigenstate throughout the evolution. For STIRAP, the system is prepared in the dark state at the initial time t_i ($|\Psi(t_i)\rangle = |\Phi^{(0)}(t_i)\rangle$). To achieve this, the pulse ordering must be counter-intuitive: the Stokes pulse must precede the pump pulse. At the initial time, $\Omega_p(t_i) \ll \Omega_S(t_i)$, so $\theta(t_i) \to 0$ and:

$$|\Phi^{(0)}(t_i)\rangle \to |1\rangle. \tag{8}$$

At the final time t_f, the pump pulse dominates: $\Omega_p(t_f) \gg \Omega_S(t_f)$, so $\theta(t_f) \to \pi/2$ and:

$$|\Phi^{(0)}(t_f)\rangle \to -|3\rangle. \tag{9}$$

Thus, if the system evolves adiabatically, the population is completely transferred from $|1\rangle$ to $|3\rangle$ without ever populating $|2\rangle$:

$$|\Psi(t_i)\rangle = |1\rangle \quad \longrightarrow \quad |\Psi(t_f)\rangle = |3\rangle. \tag{10}$$

The adiabatic condition requires that the pulse areas are sufficiently large:

$$\int \Omega_p(t)dt \gg 1, \qquad \int \Omega_S(t)dt \gg 1, \tag{11}$$

and that the pulses overlap sufficiently. In practice, this is satisfied when the pulse duration is much longer than the inverse of the Rabi frequencies.

C. The five-state system

For a five-state ladder-type nuclear system (Fig. 3), the states $|1\rangle$, $|2\rangle$, $|3\rangle$, $|4\rangle$, and $|5\rangle$ are coupled sequentially via four XFEL pulses. The pump pulse couples $|1\rangle \leftrightarrow |2\rangle$, two intermediate pulses couple $|2\rangle \leftrightarrow |3\rangle$ and $|3\rangle \leftrightarrow |4\rangle$, and the Stokes pulse couples $|4\rangle \leftrightarrow |5\rangle$. The resonance condition Eq. (3) is assumed to hold for each transition.

Within the rotating wave approximation and in the interaction picture, the Hamiltonian for the five-state system takes the form:

$$H^{(5)}(t) = \frac{\hbar}{2}\begin{pmatrix} 0 & \Omega_p(t) & 0 & 0 & 0 \\ \Omega_p(t) & 0 & \Omega_{23}(t) & 0 & 0 \\ 0 & \Omega_{23}(t) & 0 & \Omega_{34}(t) & 0 \\ 0 & 0 & \Omega_{34}(t) & 0 & \Omega_S(t) \\ 0 & 0 & 0 & \Omega_S(t) & 0 \end{pmatrix}, \tag{12}$$

where $\Omega_p(t)$, $\Omega_{23}(t)$, $\Omega_{34}(t)$, and $\Omega_S(t)$ are the time-dependent Rabi frequencies associated with each laser pulse. The chain-STIRAP technique extends the standard STIRAP concept from three-state to multi-state ladder systems. In our five-state configuration, the goal is to transfer population from $|1\rangle$ to $|5\rangle$ through a sequence of four overlapping XFEL pulses, without populating intermediate states $|2\rangle$, $|3\rangle$, and $|4\rangle$. The dark state for this five-state system, which contains no contributions from $|2\rangle$ and $|4\rangle$, is:

$$|\Phi^{(0)}(t)\rangle = \mathcal{N}\left[|1\rangle - \frac{\Omega_p(t)}{\Omega_{34}(t)}|3\rangle + \frac{\Omega_p(t)\Omega_{34}(t)}{\Omega_S(t)\Omega_{23}(t)}|5\rangle\right], \tag{13}$$

where $\mathcal{N}$ is a normalization factor. This dark state contains no contributions from $|2\rangle$ and $|4\rangle$, which are the states directly coupled to the laser fields. The presence of $|3\rangle$ in the dark state might initially appear problem-

atic, but its coefficient can be suppressed by making the intermediate pulses significantly stronger than the pump and Stokes pulses.

For both three-state and five-state systems, complete population transfer requires two conditions to be satisfied. First, the system must initially coincide with the dark state. For the three-state system, this requires $\Omega_p(t_i)/\Omega_S(t_i) \to 0$ at the initial time t_i, which is achieved by the counter-intuitive pulse ordering where the Stokes pulse precedes the pump pulse. For the five-state system, we additionally require $\Omega_p(t_i)/\Omega_{34}(t_i) \to 0$ and finite $\Omega_{23}(t_i)$, which is achieved by having the intermediate and Stokes pulses precede the pump pulse.

Second, the temporal evolution must be sufficiently slow so that the system remains in the dark state throughout the interaction. This adiabatic condition is satisfied when the pulse areas are sufficiently large, i.e., $\int \Omega_i(t)dt \gg 1$ for all pulses.

For the five-state system, an additional condition is required to prevent population of the intermediate state $|3\rangle$: the peak Rabi frequencies of the intermediate pulses(Ω_{0ij}) should be much larger than those of the pump and Stokes pulses:

$$\Omega_{023} = \Omega_{034} \gg \Omega_{0p} = \Omega_{0S}. \tag{14}$$

Under these conditions, both systems follow their respective dark states adiabatically. The three-state system starts as $|1\rangle$ and ends as $|3\rangle$, while the five-state system starts as $|1\rangle$ and ends as $|5\rangle$, without ever populating the intermediate states significantly.

D. Rabi frequency expressions

The Rabi frequencies are determined by the laser and nuclear parameters. For a transition between states $|i\rangle$ and $|j\rangle$ with multipolarity L_{ij}, the peak Rabi frequency in the nuclear rest frame is given by:

$$\Omega_{0ij} = \left[\frac{\gamma^2(1+\beta\cos\theta_{ij})^2(L_{ij}+1)(2I_i+1)B(\sigma L_{ij})}{c\epsilon_0 L_{ij}}\right]^{1/2} \times \frac{4\sqrt{\pi}}{\hbar}\frac{k_{ji}^{L_{ij}-1}}{(2L_{ij}+1)!!}, \tag{15}$$

where I_i is the angular momentum of the initial state, $B(\sigma L_{ij})$ is the reduced transition probability ($\sigma = E$ for electric or $\sigma = M$ for magnetic transitions), k_{ji} is the wave number, and the double factorial accounts for geometric factors. The effective laser intensity entering the Rabi frequency includes the Doppler enhancement and the finite bandwidth of the XFEL source.

Assuming Gaussian temporal profiles for all pulses with equal duration T, the time-dependent Rabi frequencies for the three-state system are:

$$\Omega_p(t) = \Omega_{0p}\exp\left[-\left(\frac{t-\tau_p}{\tilde{T}_p}\right)^2\right], \tag{16}$$

$$\Omega_S(t) = \Omega_{0S}\exp\left[-\left(\frac{t-\tau_S}{\tilde{T}_S}\right)^2\right], \tag{17}$$

and for the five-state system:

$$\Omega_p(t) = \Omega_{0p}\exp\left[-\left(\frac{t-\tau_p}{\tilde{T}_p}\right)^2\right], \tag{18}$$

$$\Omega_{23}(t) = \Omega_{023}\exp\left[-\left(\frac{t-\tau_{23}}{\tilde{T}_{23}}\right)^2\right], \tag{19}$$

$$\Omega_{34}(t) = \Omega_{034}\exp\left[-\left(\frac{t-\tau_{34}}{\tilde{T}_{34}}\right)^2\right], \tag{20}$$

$$\Omega_S(t) = \Omega_{0S}\exp\left[-\left(\frac{t-\tau_S}{\tilde{T}_S}\right)^2\right], \tag{21}$$

where $\tilde{T}_{ij} = \sqrt{2}T/[\gamma(1+\beta\cos\theta_{ij})]$ is the effective pulse duration in the nuclear rest frame, and τ_{ij} denote the temporal peak positions.

E. Quantum battery performance metrics

To evaluate the performance of our nuclear system as a quantum battery, we introduce several key figures of merit that quantify the energy storage and extraction capabilities. Unlike classical batteries where stored energy is directly accessible, quantum systems impose fundamental constraints on the maximum extractable work due to quantum correlations and coherence.

1. Stored energy

The total energy stored in the quantum battery at time t is defined as the expectation value of the system Hamiltonian relative to the ground state energy. For our five-state nuclear system with Hamiltonian $H = \sum_{i=1}^{5} E_i|i\rangle\langle i|$, the stored energy is:

$$E_{\text{stored}}(t) = \text{Tr}[H\rho(t)] - E_1 = \sum_{i=1}^{5} E_i\rho_{ii}(t) - E_1, \tag{22}$$

where $\rho(t)$ is the density matrix of the system and $\rho_{ii}(t)$ are the populations of each nuclear state. This quantity represents the total energy deposited in the battery during the charging process. The maximum possible stored energy is achieved when the entire population resides in the highest state $|5\rangle$, yielding $E_{\text{stored}}^{\max} = E_5 - E_1$.

2. Ergotropy

Not all stored energy can be converted into useful work. The maximum amount of work that can be extracted from a quantum system by means of cyclic unitary operations is called ergotropy. For a system with Hamiltonian H and density matrix ρ, the ergotropy is defined as:

$$\mathcal{E}(t) = \mathrm{Tr}[H\rho(t)] - \min_U \mathrm{Tr}[HU\rho(t)U^\dagger], \tag{23}$$

where the minimization is performed over all unitary transformations U. The minimizing state, denoted ρ_{passive}, is the passive state that yields the smallest energy for a given entropy. For a system with non-degenerate energy levels ordered as $E_1 < E_2 < \cdots < E_5$, the passive state is obtained by sorting the eigenvalues of $\rho(t)$ in descending order and assigning them to the energy levels in ascending order.

Let $r_1(t) \geq r_2(t) \geq \cdots \geq r_5(t)$ be the eigenvalues of $\rho(t)$ sorted in decreasing order. The ergotropy is then given by:

$$\mathcal{E}(t) = \sum_{i=1}^{5} E_i \left(\rho_{ii}^{\mathrm{ord}}(t) - r_i(t)\right), \tag{24}$$

where $\rho_{ii}^{\mathrm{ord}}(t)$ are the diagonal elements of $\rho(t)$ after applying the same permutation that sorts the eigenvalues. For a pure state undergoing unitary evolution, the ergotropy simplifies to:

$$\mathcal{E}(t) = \sum_{i=1}^{5} E_i |c_i(t)|^2 - E_1, \tag{25}$$

where $c_i(t)$ are the probability amplitudes, provided the state remains pure during the charging process. This is the case for our coherent chain-STIRAP protocol in the absence of dissipation.

The ergotropy satisfies $0 \leq \mathcal{E}(t) \leq E_{\mathrm{stored}}(t)$. The upper bound is reached when the system is in a pure state with no population inversion relative to the passive state ordering, i.e., when higher energy levels have higher populations.

3. Charging efficiency

The charging efficiency quantifies how much of the stored energy is actually extractable as work. It is defined as the ratio of ergotropy to stored energy:

$$\eta(t) = \frac{\mathcal{E}(t)}{E_{\mathrm{stored}}(t)}. \tag{26}$$

Ideal charging corresponds to $\eta = 1$, where all stored energy can be extracted. Values less than unity indicate that some energy is locked in correlations that cannot be converted into work by unitary operations. In the context of nuclear batteries, maximizing η is crucial for practical applications.

4. Charging power

The average charging power represents the rate at which energy is stored in the battery. It is defined as:

$$P = \frac{\mathcal{E}(T_{\mathrm{charge}})}{T_{\mathrm{charge}}}, \tag{27}$$

where T_{charge} is the duration of the charging process, typically taken as the time when ergotropy reaches its maximum value. High power is desirable for rapid energy delivery, though there exists a fundamental trade-off between power and efficiency in quantum systems.

In the following section, we will compute these quantities for both three-state and five-state nuclear systems charged via STIRAP and chain-STIRAP protocols, respectively, using ^{168}Er nuclear parameters.

III. NUMERICAL FRAMEWORK

A. Nuclear and Laser parameters for numerical simulation

For concrete numerical calculations, we employ two different nuclei to investigate the three-state and five-state systems separately. This choice is motivated by the availability of suitable level schemes and the desire to benchmark our results with existing experimental data.

For the three-state benchmark system, we utilize the ^{223}Ra and ^{168}Er nucleus. The selected low-lying levels form a rotational band with a well-defined E2 cascade. In the ^{223}Ra, the ground state $|1\rangle$ has spin-parity $3/2^+$, while the excited states $|2\rangle$ and $|3\rangle$ have spins $7/2^+$ and $9/2^+$, respectively. The transition energies are $E_2 = 61.42$ keV and $E_3 = 174.57$ keV. The lifetimes of the excited states are sufficiently long (on the order of nanoseconds) compared to the XFEL pulse duration, ensuring that spontaneous decay does not affect the coherent dynamics during the charging process. The relevant nuclear parameters for ^{223}Ra and ^{168}Er are summarized in Table I.

For the five-state system, we employ the ^{168}Er nucleus, which has been extensively studied in the context of nuclear quantum optics and coherent population transfer. The low-lying spectrum of ^{168}Er forms a rotational band with energies $E_1 = 0$ keV (ground state), $E_2 = 79.8$ keV, $E_3 = 264.09$ keV, $E_4 = 548.75$ keV, and $E_5 = 928.30$ keV. All transitions between consecutive states are of electric quadrupole (E2) type with multipolarity $L_{ij} = 2$. The reduced transition probabilities $B(E2)$ are calculated using the Weisskopf single-particle estimate, which provides a good approximation for collective nuclear transitions. The lifetimes of the excited states range from several picoseconds to nanoseconds, which is orders of magnitude longer than the duration of the XFEL pulses (approximately 100 fs in the laboratory frame). Therefore, spontaneous emission and other

TABLE I. Nuclear parameters. E_i is the energy of state $|i\rangle$ with $i \in 1, 2, 3$ (in keV). The spin of ground state $|1\rangle$, multipolarities, reduced matrix elements (in Weisskopf units, wsu) for the transitions $|1\rangle \to |2\rangle$, $|2\rangle \to |3\rangle$ and also the lifetime of excited states are given for ^{223}Ra and ^{168}Er.

Nucli	E_1	E_2	E_3	I_1	I_2	$\epsilon/\mu L_{21}$	$\epsilon/\mu L_{32}$	L_{21}	L_{32}	B($\varepsilon/\mu L_{21}$) (wsu)	B($\varepsilon/\mu L_{32}$) (wsu)	$T^{(21)}_{\frac{1}{2}}(s)$	$T^{(32)}_{\frac{1}{2}}(s)$
^{223}Ra	0.0	61.424	174.569	$\frac{3}{2}^+$	$\frac{7}{2}^+$	E2	E2	2	2	44	280	0.6×10^{-9}	0.2×10^{-9}
^{168}Er	0.0	79.80	264.09	0^+	2^+	E2	E2	2	2	213	319	1.853×10^{-9}	1.4×10^{-12}

dissipative processes are completely negligible during the charging process, justifying the use of a closed quantum system model. The relevant parameters for ^{168}Er are listed in Table II.

To realize the proposed population transfer schemes, we require X-ray free-electron laser pulses with specific characteristics. The parameters of the laser pulses play a crucial role in the efficiency and feasibility of both STIRAP and chain-STIRAP protocols. We assume that all laser pulses have identical Gaussian temporal profiles in the laboratory frame. For our numerical simulations, we set the pulse duration to $T = 10^{-13}$ s in the laboratory frame, which is consistent with the parameters of the European XFEL facility and similar sources. This duration is sufficiently short compared to the nuclear excited state lifetimes but sufficiently long to satisfy the adiabatic condition for STIRAP. Due to the relativistic Doppler effect, the pulse duration is transformed in the nuclear rest frame. This shortening of the pulse duration in the nuclear rest frame is beneficial for achieving high peak Rabi frequencies and satisfying the adiabatic condition.

The laser parameters used in our simulations are consistent with the specifications of existing and planned XFEL facilities, such as the European XFEL, the Linac Coherent Light Source (LCLS), and the Shanghai XFEL (SXFEL). Key parameters include:

- Photon energy range: up to 25 keV
- Pulse duration: 10^{-14} to 10^{-13} s
- Peak power: up to 100 GW
- Focused spot size: down to ~ 10 nm
- Peak intensity: up to 10^{22} W/cm^2 (current) and up to 10^{26} W/cm^2 (with focusing)
- Bandwidth: ~ 10 meV to 1 eV

Due to the finite bandwidth of the XFEL, not all photons can effectively drive the nuclear transition. The effective laser intensity is reduced by the ratio of the nuclear linewidth to the laser bandwidth ($I^{\text{eff}}_{ij} = I_{ij}\frac{\Gamma_{ij}}{\Gamma'}$). where Γ_{ij} is the natural linewidth of the nuclear transition and Γ' is the laser bandwidth. For the high-γ regime where the nuclear linewidth exceeds the laser bandwidth, the effective intensity equals the nominal intensity. For our parameters with ^{168}Er, the nuclear linewidths are on the order of 10^{-6} eV, which is smaller than the XFEL bandwidth of approximately 10 meV. This results in a reduction factor of approximately 10^{-4}, meaning that the effective intensity is much lower than the nominal intensity. To overcome this reduction, we operate in the regime where the Doppler-broadened linewidth exceeds the laser bandwidth. The Doppler broadening in the nuclear rest frame is:

$$\Gamma_{\text{Doppler}} = \gamma(1+\beta)\Gamma'. \tag{28}$$

The suggested laser that can be used in this study is SXFEL with the Laser photon energy of 12.4 keV, also $\Gamma = 10meV$ is laser bandwidth and the pulse duration of laser in the laboratory frame is 0.1 ps. The population completely reversed to the excited state in three-state systems by adjusting the laser and nuclear beam parameters as Table III.

For the five-state system, the laser parameters must satisfy the chain-STIRAP conditions. The resonance condition is according to Eq. (3), and the required Rabi frequencies are computed using Eq. (15). To achieve complete population transfer from $|1\rangle$ to $|5\rangle$, the pulse sequence must follow the counter-intuitive ordering such that the Stokes and intermediate pulses precede the pump pulse. We suggested SXFEL with the Laser photon energy of 20.7 keV for five-state system complete population transfer. So, by the use of the resonance condition, we calculated $\theta_p = 134.83°$, $\theta_{23} = 108.33°$, $\theta_{34} = 52.78°$, and $\theta_S = 0.0°$.

We assume Gaussian temporal profiles for all four pulses with equal duration in the laboratory frame. The Lorentz factor($\gamma = 12.97$) and pulse durations are chosen such that the adiabatic condition is satisfied while the Doppler-shifted laser frequencies match the nuclear transition energies. Considering $T = 10^{-13}$, we determined $\tilde{T}_p = 36.68 \times 10^{-15}s$, $\tilde{T}_{23} = 15.88 \times 10^{-15}s$, $\tilde{T}_{34} = 10.28 \times 10^{-15}s$, and $\tilde{T}_S = 5.46 \times 10^{-15}s$. The intensity of each pulse($I_p = 1.2076 \times 10^{+28}$, $I_{23} = 10.7402 \times 10^{+26}$, $I_{34} = 3.059 \times 10^{+25}$, and $I_S = 2.2576 \times 10^{+23} W.cm^{-2}$) is determined by the corresponding Rabi frequency required for complete population transfer.

The intermediate pulses (Ω_{23} and Ω_{34}) require significantly higher intensities than the pump and Stokes pulses. where $\Omega_{23} = \Omega_{34} = m\Omega_p$. This ensures that the coefficient of $|3\rangle$ in the dark state is suppressed, preventing population trapping in the intermediate state. For the mentioned parameters, the enhancement factor is approximately $m = 5$.

The temporal peak positions are set as $\tau_p = \tau_S = 1.53 \times 10^{-14}$ s and $\tau_{23} = \tau_{34} = 0.7\tau_p$, ensuring that the

TABLE II. Nuclear parameters for the five-state system of ^{168}Er. The energies E_i, spins I_i, multipolarities L_{ij}, and reduced transition probabilities $B(\varepsilon/\mu L_{32})$ (in Weisskopf units) are given for all four transitions.

E_1	E_2	E_3	E_4	E_5	I_1	I_2	I_3	I_4	$\epsilon/\mu L_{21}$	$\epsilon/\mu L_{32}$	$\epsilon/\mu L_{43}$	$\epsilon/\mu L_{54}$	B($\varepsilon/\mu L_{21}$)	B($\varepsilon/\mu L_{32}$)	B($\varepsilon/\mu L_{43}$)	B($\varepsilon/\mu L_{54}$)
0.0	79.80	264.09	548.75	928.30	0^+	2^+	4^+	26^+	E2	E2	E2	E2	213	319	424	354

TABLE III. Adjusted parameters in the interaction of three-state nuclei with the laser for complete population transmission in the STIRAP method.

Nucli	γ	$\tilde{T}_p(fs)$	$\tilde{T}_S(fs)$	$I_p(W.cm^{-2})$	$I_S(W.cm^{-2})$	θ_p	θ_S
^{223}Ra	4.61	28.5	15.5	20.76×10^{24}	3.36×10^{24}	85.6°	0.0°
^{168}Er	7.46	21.9	9.51	32.25×10^{27}	7.32×10^{23}	98.0°	0.0°

intermediate and Stokes pulses precede the pump pulse. The pulse durations T_{ij} are equal for all four pulses in the laboratory frame, and the effective durations in the nuclear rest frame are shortened by the relativistic Doppler factor.

B. Numerical results

In this section, we present the numerical results for both three-state and five-state nuclear systems. The time-dependent Schrödinger equation is solved using the Hamiltonians given in Eqs. (4) and (12) with the parameters listed before. All simulations are performed using MATLAB.

We first analyze the three-state system using the STIRAP protocol. Figure 4 shows the time evolution of the Rabi frequencies and state populations for the ^{223}Ra nucleus with the parameters listed in Table I, and III. As shown in Fig. 4(b), the system starts entirely in $|1\rangle$. Following the counter-intuitive pulse ordering, the population is transferred smoothly to $|3\rangle$ without significant population of the intermediate state $|2\rangle$. At the final time, the population in $|3\rangle$ exceeds 99%, confirming complete population transfer. Figure 4(c) displays the ergotropy during the charging process. The ergotropy increases from zero to approximately 99% of the stored energy at the final time, indicating that most of the stored energy is extractable as useful work.

We now turn to the five-state system using the chain-STIRAP protocol. Figure 5(a) shows the time evolution of the four Rabi frequencies for the five-state ^{168}Er system with the parameters given in Section III.A.

Figure 5(b) shows the state populations during the chain-STIRAP process. The system starts in $|1\rangle$ and the population is sequentially transferred through the dark state manifold to $|5\rangle$. Remarkably, the intermediate states $|2\rangle$, $|3\rangle$, and $|4\rangle$ remain nearly unpopulated throughout the entire evolution. At the final time, the population in $|5\rangle$ exceeds 99%, confirming complete population transfer.

Figure 5(c) presents the stored energy and ergotropy

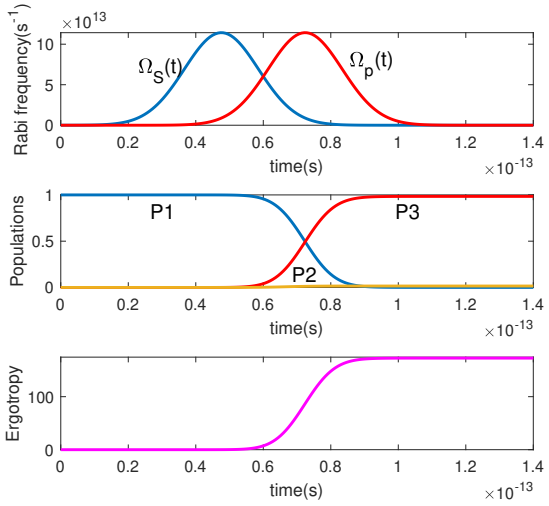


FIG. 4. Time evolution of (a) Rabi frequencies, (b) state populations, and (c) ergotropy for the three-state ^{223}Ra system driven by STIRAP. The population is completely transferred from $|1\rangle$ to $|3\rangle$ without populating $|2\rangle$. Parameters are taken from Table III.

for the five-state system. The stored energy rises to approximately $E_5 - E_1 = 928.30$ keV, which is significantly higher than the three-state case. The ergotropy reaches 99% of the stored energy, corresponding to a charging efficiency of $\eta = 0.99$.

In addition to stored energy and ergotropy, the charging power is a crucial figure of merit for practical quantum battery applications. The charging power quantifies the rate at which energy is stored in the battery and is defined as (27). For the three-state ^{223}Ra and ^{168}Er systems driven by standard STIRAP, the average charging powers are $0.279W$ and $0.423W$ respectively, which are remarkably high for a microscopic quantum system, highlighting the ultrafast nature of the STIRAP-based charging protocol.

For the five-state ^{168}Er system driven by chain-STIRAP, the charging duration is also $T^{(5)}_{charge} \sim 10^{-13}$. With a final ergotropy of $\mathcal{E}^{(5)} = 918.1keV$ (approximately 99% of the stored energy), the average charging power is $1.47W$, which is more than 30 times higher than the three-state case. This significant enhancement in charging power arises from two factors: (i) the larger energy gap in the five-state system, which allows for substantially higher stored energy, and (ii) the short pulse duration.

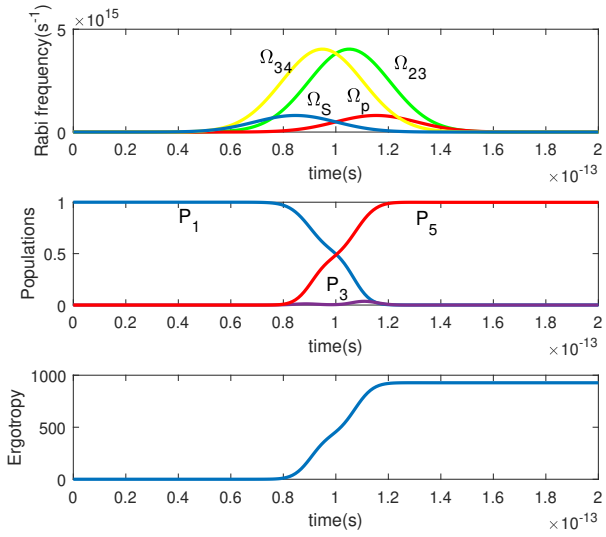


FIG. 5. Time evolution of (a) the four Rabi frequencies Ω_p, Ω_{23}, Ω_{34}, and Ω_S for the five-state ^{168}Er system. The intermediate pulses have significantly higher peak intensities than the pump and Stokes pulses. (b) populations for the five-state ^{168}Er system driven by chain-STIRAP. The population is completely transferred from $|1\rangle$ to $|5\rangle$ without populating intermediate states. (c) ergotropy as functions of time for the five-state ^{168}Er system. The final ergotropy reaches 99% of the stored energy.

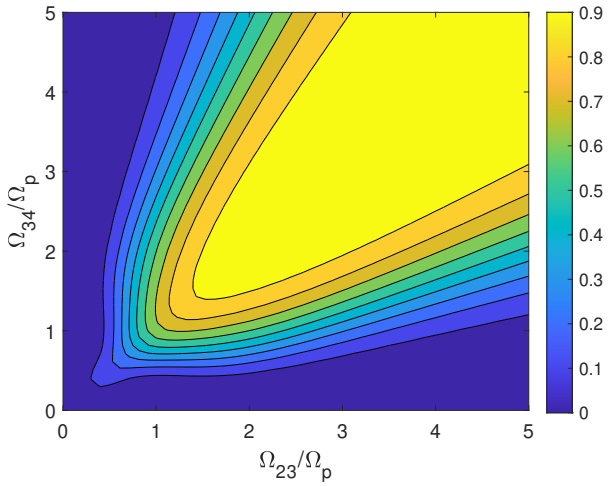


FIG. 6. Robustness analysis of the chain-STIRAP protocol for the five-state ^{168}Er system: Charging efficiency η as a function of the normalized intermediate Rabi frequencies Ω_{23}/Ω_p and Ω_{34}/Ω_p. The laser parameters are choosn as Fig. 5

C. Robustness Analysis

For any practical implementation, the sensitivity of the charging protocol to parameter fluctuations is a critical concern. Here, we systematically investigate the robustness of our chain-STIRAP scheme against variations in the key experimental parameters.

Figure 6 displays the final charging efficiency η as a function of the relative amplitudes of the intermediate pulses Ω_{23} and Ω_{34}, normalized to Ω_p. The pump and Stokes pulses are kept fixed at their optimal values. As clearly seen, the efficiency remains above 90% for a wide range of intensity variations, specifically for $\Omega_{23}/\Omega_p > 3$ and $\Omega_{34}/\Omega_p > 3$. This broad plateau confirms that the protocol is highly tolerant to fluctuations in the XFEL pulse intensities, which are typically controlled with an accuracy of better than 10% in modern facilities.

To further investigate the robustness of the chain-STIRAP protocol against timing fluctuations, we analyzed the effect of the pump pulse delay on the charging efficiency. Figure 7 shows η as a function of the normalized pump delay $\tau_p/\tilde{T}_p$ for three different configurations, characterized by the parameter $m = 3, 4, 5$. For all three configurations, the efficiency remains close to unity for small delays and decreases monotonically as $\tau_p/\tilde{T}_p$ increases. However, the m=5 configuration exhibits the broadest high-efficiency plateau, maintaining $\eta = 1$ for $0.7 < \tau_p/\tilde{T}_p < 0.85$. This behavior can be understood by noting that larger m values ensure that the intermediate pulses are sufficiently delayed relative to the pump pulse, preserving the counter-intuitive pulse ordering required for adiabatic population transfer even when the pump pulse is significantly delayed. The broader plateau for m=5 makes this configuration the preferred choice for experimental implementation, as it provides greater tolerance to synchronization errors in the XFEL pulse sequence.

To determine the optimal timing sequence for the five-state chain-STIRAP protocol, we systematically varied the delay of the intermediate pulses relative to the pump pulse. Figure 8 shows the charging efficiency η as a function of the ratio τ_p/τ_{23}, where τ_p is the pump pulse delay and τ_{23} is the delay of the first intermediate pulse. For simplicity, we assumed equal spacing between all subsequent pulses: $\tau_p = \tau_S$ and $\tau_{23} = \tau_{34}$. The efficiency exhibits a clear optimal plateau, with the maximum $\eta = 1.00$ achieved in the range $3.00 < \tau_p/\tau_{23} < 3.50$. This indicates that the intermediate pulses must precede the pump pulse by approximately three times the inter-pulse spacing to satisfy the counter-intuitive pulse ordering required for adiabatic dark-state passage. For $\tau_p/\tau_{23} < 2.00$, the efficiency drops sharply because the other pulse arrives too early, destroying the dark-state condition. For $\tau_p/\tau_{23} > 4.50$, the efficiency gradually decreases due to loss of adiabaticity as the pulses become too widely separated. The broad plateau around the optimal ratio confirms the robustness of the protocol against timing fluctuations, which is a significant advantage for experimental implementations with imperfect pulse synchronization.

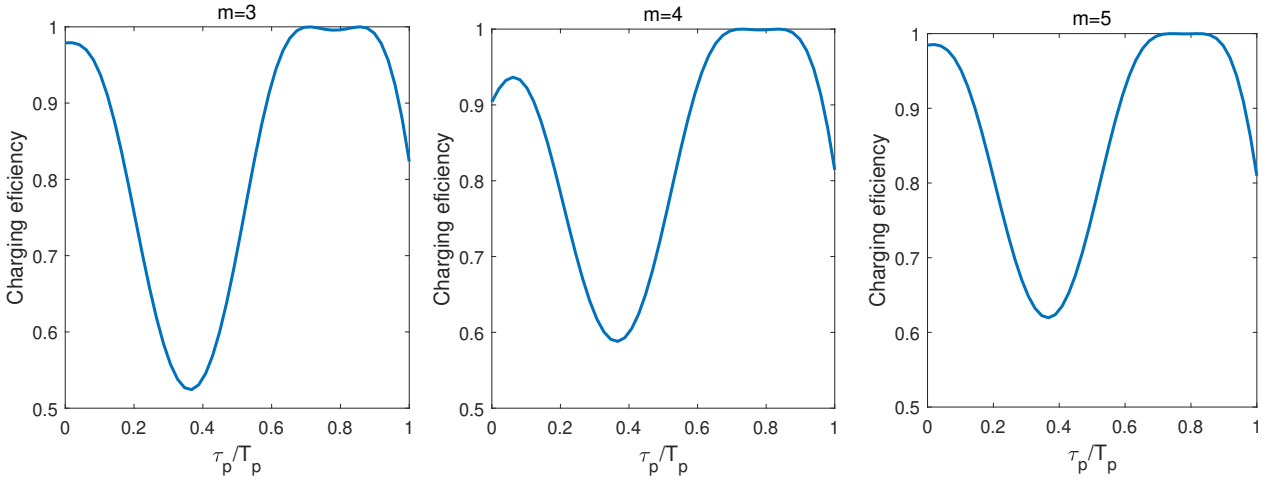


FIG. 7. Charging efficiency η versus normalized pump pulse delay $\tau_p/\tilde{T}_p$ for $m = 3, 4, 5$ of the intermediate pulses. The $m = 5$ configuration shows the best performance, maintaining $\eta = 1$ for $0.7 < \tau_p/\tilde{T}_p < 0.85$. This confirms that larger pulse spacing enhances robustness against timing errors.

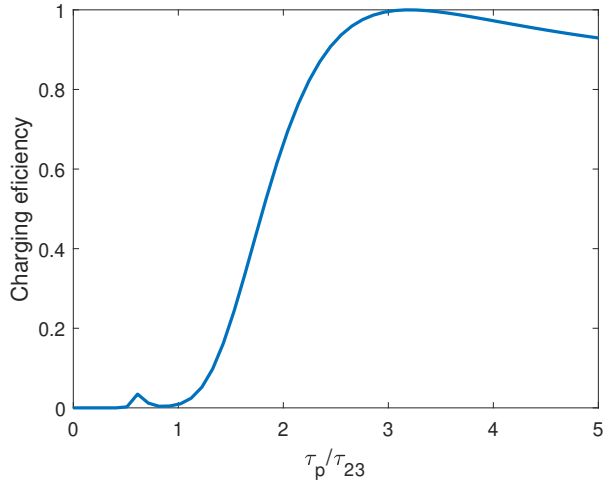


FIG. 8. Charging efficiency η versus the ratio of τ_p/τ_{23} for the five-state ^{168}Er system. The efficiency reaches a broad maximum ($\eta = 1.00$) for $3.00 < \tau_p/\tau_{23} < 3.50$. This demonstrates that the chain-STIRAP protocol is robust against timing variations and achieves complete population transfer when the intermediate pulses precede the pump pulse by an appropriate delay. The laser parameters are choosn as Fig. 5

IV. CONCLUSION

In this work, we have theoretically investigated the optimization of stored energy and ergotropy in nuclear quantum batteries charged via coherent population transfer techniques. We analyzed two distinct ladder-type nuclear systems—a three-state system using ^{223}Ra, and a five-state system using ^{168}Er—driven by STIRAP and chain-STIRAP protocols, respectively, under realistic XFEL parameters and relativistic Doppler compensation.

Our numerical simulations demonstrate that the chain-STIRAP protocol enables complete and efficient population transfer from the ground state $|1\rangle$ to the highest excited state $|5\rangle$ in the five-state system, without significant population of the intermediate states $|2\rangle$, $|3\rangle$, and $|4\rangle$. The final population in $|5\rangle$ exceeds 99%, confirming the adiabatic nature of the process. For the three-state benchmark system using ^{223}Ra, we similarly achieved complete population transfer from $|1\rangle$ to $|3\rangle$ with a final population exceeding 99%, validating the standard STIRAP implementation.

In terms of quantum battery performance, the five-state ^{168}Er system stores a maximum energy of 927.35 keV, which is approximately four times larger than the 172.72 keV stored in the three-state ^{223}Ra system. More importantly, the charging efficiency—defined as the ratio of ergotropy to stored energy—reaches $\eta = 0.99$ for the five-state system, compared to $\eta = 0.989$ for the three-state case. This indicates that nearly all of the stored energy in the five-state system is extractable as useful work, making it a highly efficient quantum battery.

The calculated average charging powers are $P^{(3)} = 0.423\,\mathrm{W}$ and $P^{(5)} = 1.47\,\mathrm{W}$ for the three-state and five-state systems, respectively. The five-state system thus delivers more than five times the charging power of the three-state system, primarily due to its larger energy gap ($E_5 - E_1 = 928.30\,\mathrm{keV}$) and the shorter pulse durations enabled by the relativistic Doppler effect. These values, while modest on an absolute scale for a single nucleus, are remarkably high when considering the microscopic volume of a single nucleus and underscore the potential of nuclear systems for ultra-dense energy storage applications.

A key advantage of our proposed scheme is the

significant reduction in required peak laser intensity. The chain-STIRAP protocol achieves complete population transfer with peak intensities on the order of $10^{26}\,\mathrm{W/cm^2}$, which is considerably lower than conventional π-pulse or standard STIRAP methods. This reduction is made possible by the use of strong intermediate pulses that suppress population in the unwanted intermediate states, as described by the dark-state condition in Eq. (13) and the condition $\Omega_{023} = \Omega_{034} \gg \Omega_{0p} = \Omega_{0S}$ in Eq. (14).

We further conducted a comprehensive robustness analysis to assess the practical feasibility of our protocol. Our results confirm that the chain-STIRAP scheme is highly tolerant to:

- **Intensity fluctuations**: The efficiency remains above 90% for a wide range of intermediate pulse intensities, specifically for $\Omega_{23}/\Omega_p > 3$ and $\Omega_{34}/\Omega_p > 3$ (Fig. 6), which is well within the intensity stability of modern XFEL facilities.
- **Timing errors**: The $m = 5$ configuration maintains $\eta = 1$ for $0.7 < \tau_p/\tilde{T}_p < 0.85$ (Fig. 7), demonstrating excellent tolerance to pump pulse timing fluctuations.
- **Pulse synchronization**: Optimal performance is achieved for $3.0 < \tau_p/\tau_{23} < 3.5$, with a broad plateau ensuring tolerance to synchronization errors (Fig. 8).

This robustness, inherent to the adiabatic dark-state passage, makes the chain-STIRAP protocol a practical candidate for experimental implementation with current and next-generation XFEL facilities.

In summary, our work establishes chain-STIRAP as a powerful and practical tool for charging high-capacity nuclear quantum batteries. The combination of high energy density (nearly 1 MeV per nucleus), near-unity charging efficiency ($\eta = 0.99$), enhanced charging power ($P^{(5)} = 1.47\,\mathrm{W}$ per nucleus), and robustness against parameter fluctuations positions nuclear quantum batteries as a promising platform for future energy storage technologies.

Future research directions include the extension of our protocol to higher-order chain systems with more than five states, which could further increase the stored energy and potentially approach the MeV scale. Additionally, the inclusion of dissipative effects, decoherence, and finite-temperature environments in the theoretical model would provide a more realistic assessment of battery performance under experimental conditions. Finally, exploring collective charging effects in ensembles of nuclei could potentially enhance both the power and energy capacity through quantum entanglement and cooperative interactions, offering a pathway toward macroscopic nuclear quantum batteries.

The convergence of nuclear physics, quantum optics, and quantum battery technology opens new frontiers for ultra-dense, long-lasting, and rapidly chargeable power sources, with potential applications in space missions, medical devices, and other critical sectors requiring compact and reliable energy storage.

CONFLICT OF INTEREST STATEMENT

The authors declare no competing interests.

FUNDING INFORMATION

This research received no specific grant from any funding agency in the public, commercial, or not-for-profit sectors.

DATA AVAILABILITY

The data that support the findings of this study are available from the corresponding author upon reasonable request.

[1] L. Allen and J. H. Eberly, *Optical Resonance and Two-Level Atoms* (Wiley, New York, 1975).
[2] B. W. Shore, *The Theory of Coherent Atomic Excitation* (Wiley, New York, 1990).
[3] K. Bergmann, N. V. Vitanov, and B. W. Shore, J. Chem. Phys. **142**, 170901 (2015).
[4] U. Gaubatz, P. Rudecki, S. Schiemann, and K. Bergmann, J. Chem. Phys. **92**, 5363 (1990).
[5] N. V. Vitanov, M. Fleischhauer, B. W. Shore, and K. Bergmann, Adv. At. Mol. Opt. Phys. **46**, 55 (2001).
[6] N. V. Vitanov, A. A. Rangelov, B. W. Shore, and K. Bergmann, Rev. Mod. Phys. **89**, 015006 (2017).
[7] N. V. Vitanov, Phys. Rev. A **58**, 2295 (1998).
[8] V. S. Malinovsky and D. J. Tannor, Phys. Rev. A **56**, 4929 (1997).
[9] I. R. Sola, V. S. Malinovsky, and D. J. Tannor, Phys. Rev. A **60**, 3081 (1999).
[10] N. V. Vitanov, J. Phys. B: At. Mol. Opt. Phys. **33**, 233 (2000).
[11] A. Pálffy, J. Mod. Opt. **55**, 2603 (2008).
[12] A. Pálffy, C. H. Keitel, and J. Evers, Phys. Rev. B **83**, 155103 (2011).
[13] W. T. Liao, *Coherent Control of Nuclei and X-Rays* (Springer, Cham, 2014) pp. 27-48.
[14] T. J. Bürvenich, J. Evers, and C. H. Keitel, Phys. Rev. Lett. **96**, 142501 (2006).
[15] W. T. Liao, A. Pálffy, and C. H. Keitel, Phys. Rev. C **87**, 054609 (2013).
[16] T. Kirschbaum, N. Minkov, and A. Pálffy, Phys. Rev. C **105**, 064313 (2022).

[17] B. Nedaee-Shakarab, M. Saadati-Niari, and F. Zolfagharpour, Phys. Rev. C **94**, 054601 (2016).
[18] N. Mansourzadeh-Ashkani, M. Saadati-Niari, F. Zolfagharpour, and B. Nedaee-Shakarab, Nucl. Phys. A **1007**, 122119 (2021).
[19] M. Amiri and M. Saadati-Niari, Eur. Phys. J. A **59**, 32 (2023).
[20] M. Amiri and M. Saadati-Niari, Phys. Scr. **98**, 085303 (2023).
[21] F. Binder, L. A. Correa, C. Gogolin, J. Anders, and G. Adesso, *Fundamental Theories of Physics* **195**, 1 (2018).
[22] F. Campaioli, F. A. Pollock, F. C. Binder, L. Céleri, J. Goold, S. Vinjanampathy, and K. Modi, Phys. Rev. Lett. **118**, 150601 (2017).
[23] R. Alicki and M. Fannes, Phys. Rev. E **87**, 042123 (2013).
[24] D. Ferraro, M. Campisi, G. M. Andolina, V. Pellegrini, and M. Polini, Phys. Rev. Lett. **120**, 117702 (2018).
[25] G. M. Andolina, M. Keck, A. Mari, M. Campisi, V. Giovannetti, and M. Polini, Phys. Rev. Lett. **122**, 047702 (2019).
[26] S. Zakavati, F. T. Tabesh, and S. Salimi, Phys. Rev. E **104**, 054117 (2021).
[27] K. V. Hovhannisyan, M. Perarnau-Llobet, M. Huber, and A. Acín, Phys. Rev. Lett. **111**, 240401 (2013).
[28] F. T. Tabesh, F. H. Kamin, and S. Salimi, Phys. Rev. A **102**, 052223 (2020).
[29] F. H. Kamin, F. T. Tabesh, S. Salimi, F. Kheirandish, and A. C. Santos, Phys. Rev. E **102**, 052109 (2020).
[30] M. Carrega, A. Crescente, D. Ferraro, and M. Sassetti, New J. Phys. **22**, 083085 (2020).